

Cite this: *Soft Matter*, 2012, **8**, 4343

www.rsc.org/softmatter

PAPER

Novel “soft” biodegradable nanoparticles prepared from aliphatic based monomers as a potential drug delivery system†

Alessandro Jäger,^{*a} Daniel Gromadzki,^a Eliézer Jäger,^a Fernando Carlos Giacomelli,^b Agnieszka Kozłowska,^c Libor Kožbera,^a Jiří Brus,^a Blanka Říhová,^d Mirosława El Fray,^c Karel Ulbrich^a and Petr Štěpánek^{*a}

Received 24th November 2011, Accepted 6th February 2012

DOI: 10.1039/c2sm07247e

The search for new biomaterials intended for biomedical applications has considerably intensified in recent years. Herein, the synthesis and characterization of a new aliphatic biodegradable copolyester named PBS/PBDL (poly(butylene succinate-*co*-butylene dilinoleate)) is reported. Surfactant-free, narrowly distributed, nanosized spherical particles ($R_H < 60$ nm) have been produced from the biodegradable material by applying a single-step nanoprecipitation protocol. Their structure was characterized in detail by employing a variety of scattering techniques and transmission electron microscopy (TEM). Combined SLS and DLS measurements suggested that the nanoparticles comprise a porous core conferring a non-compact characteristic. Their porosity enables water to be entrapped which is responsible for their pronounced stability and relatively fast degradation as followed by size exclusion chromatography (SEC). The polymeric nanoparticles could be loaded with the hydrophobic model drug paclitaxel (PTX) with an encapsulation efficiency of ~95% and drug loading content of ~6–7% $w_{\text{drug}}/w_{\text{polymer}}$. The drug release was followed by HPLC and scattering measurements (DLS, SLS and SAXS). The drug encapsulation and release modifies the inner structure of the nanoparticles, which holds a large amount of entrapped water in the drug-free condition. PTX encapsulation leads to replacement of the entrapped water by the hydrophobic model drug and to shrinking of the nanoparticles, probably due to favorable drug–polymer hydrophobic interactions. Cell viability experiments demonstrated that the nanoparticles are biocompatible and non-toxic, making them potentially useful for applications in nanomedicine.

1. Introduction

The use of pharmaceutical polymeric nanocarriers has become one of the most important areas of nanomedicine. Particularly, the manufacturing of efficient drug delivery systems that enable drug targeting and specific delivery of difficult-to-deliver molecules has been extensively investigated.^{1,2} Thanks to the advances in polymer chemistry and polymer colloids, it is now possible to prepare polymeric nanoparticles with unique, finely tuned

properties that are required to achieve the goal of drug targeting.^{3–5}

Over the past decades, the use of biodegradable polymers in the preparation of pharmaceutical formulations and biomedical devices has increased dramatically. Among these the most promising applications are the ones focused on the development of controlled drug delivery systems.^{6,7} The use of biodegradable polymers is very attractive because controlled drug release can be optimized by suitable degradation strategies and it allows clearance of the polymeric material from the body, avoiding its accumulation and possible toxicity.^{8,9} Nevertheless, the available biodegradable polymers that are suitable for biomedical applications are limited due to the essential requirement of biocompatibility. Furthermore, the degradation mechanism must also not lead to the formation of poisonous products.¹⁰

Among the FDA-approved polymers, the aliphatic polyesters such as poly(ϵ -caprolactone) (PCL), polylactic acid (PLA) and poly(lactic-*co*-glycolic acid) (PLGA) have been extensively and routinely used in the manufacturing of drug delivery devices¹¹ because of their good hydrolyzability, biocompatibility and drug release properties.^{9,12} In addition, polybutylene succinate (PBS) is also an important commercially available

^aInstitute of Macromolecular Chemistry, Academy of Sciences of the Czech Republic, Heyrovsky Sq. 2, 162 06 Prague 6, Czech Republic. E-mail: jager@imc.cas.cz; stepanek@imc.cas.cz; Tel: +420 296 809211; +420 296 809322

^bCentro de Ciências Naturais e Humanas, Universidade Federal do ABC, 09210-170 Santo André, Brazil

^cDivision of Biomaterials and Microbiological Technologies Polymer Institute, West Pomeranian University of Technology Szczecin, ul. Pulaskiego 10, 70-322 Szczecin, Poland

^dInstitute of Microbiology, Academy of Sciences of the Czech Republic, v. v. i., Vídeňská 1083, 142 20 Prague 4, Czech Republic

† Electronic supplementary information (ESI) available. See DOI: 10.1039/c2sm07247e

biodegradable aliphatic polyester derived from fatty C-4 compounds.^{13–15} Recently, its copolymerization with different comonomers led to novel biomedical materials exhibiting particular biodegradation behaviors and good biocompatibility.^{16–18} The absence of cytotoxic degradation products, *e.g.* succinic acid is an intermediate in the TCA cycle (tricarboxylic acid cycle, citric acid cycle), makes PBS copolyesters prospective candidates aiming the development of drug delivery structures.¹⁹ Furthermore, fatty acids (FA) are suitable components for the preparation of biodegradable polymers since they are hydrophobic compounds that naturally occur in the body. Consequently, they might retain encapsulated hydrophobic drugs *via* hydrophobic interactions when used as drug nanocarriers.²⁰ Heretofore, different fatty acid monomers obtained from natural sources have been suggested as starting materials to produce devices focusing on biomedical applications.²¹ Among those, dilinoleic acid (DLA) is dimerized linoleic acid and it is a suitable monomer for step growth polycondensation resulting in copolymers of numerous structures.^{22–25} Recently, multiblock copolymers containing DLA monomer units were proposed as biomaterials for bone and tissue engineering that demonstrated good biocompatibility.^{26,27} Although copolymers containing FA monomers as building blocks were extensively proposed in the literature as devices in many biomedical applications, their application as nanocarriers for drug release was not reported to date. Hence, DLA copolymer-based biodegradable and biocompatible polyesters can render very interesting biomaterials that are useful as nanocarriers and they deserve to be investigated for such a purpose.

Herein a new biodegradable and biocompatible copolyester composed of succinic acid (SA), butanediol (BD) and DLA as building block monomers is proposed for the production of polymeric nanocarriers. The copolyester was synthesized by environmentally benign melt polycondensation²⁸ using commercially available “green” monomers and characterized in detail by employing standard techniques. By using the novel copolyester, sub-120 nm surfactant-free nanocarriers have been prepared by a well-known nanoprecipitation protocol. The nanoprecipitation constitutes an easy and reproducible procedure that has been widely used in the preparation of polyester-based nanoparticles.^{9,29,30} Among its advantages are: *i*) large amounts of hazardous solvents are avoided; *ii*) narrowly distributed nanosized spherical particles can be obtained; *iii*) external energy sources are unnecessary and *iv*) the process can be easily scaled-up.^{9,31,32} Their biodegradability, biocompatibility and controlled drug release properties have been further verified by using paclitaxel (PTX) as the model drug. The drug encapsulation and drug release changes the inner structure of the polymeric nanoparticles and this issue has been deeply detailed and discussed throughout the manuscript.

2. Experimental

2.1 Materials and reagents

Dilinoleic acid (DLA) Pripol 1009 (Croda Coatings & Polymers), 1,4-butanediol (BD) (BASF), succinic acid (SA) (Aldrich Chemie) and acetone (Merck) were used as received. The water consumed was ultrapure MilliQ®.

2.2 Synthesis of the copolyester

The copolyester PBS/PBDL was synthesized by the typical melt polycondensation protocol.²⁸ The procedures were carried out on a stainless steel pressure-vacuum reactor. The esterification was conducted under vigorous stirring in presence of a magnesium–titanate organometallic complex (Mg–Ti) as catalyst and upon preset temperature ramping from 100 °C to 200 °C (heating rate = 1.5 °C min⁻¹). The reaction was stopped when the acid value was less than 2 mg KOH g⁻¹.

The polycondensation reaction was carried out at 245–250 °C, ~0.4 hPa and in the presence of the Mg–Ti catalyst. The reaction was considered complete when the observed power consumption of the stirrer motor signaled that the polymer had obtained the highest melt viscosity. The reaction mass was extruded by means of compressed nitrogen. The copolyester was purified by dissolution in chloroform and further precipitation in methanol. The poly(butylene succinate-*co*-butylene dilinoleate) herein referred to as PBS/PBDL was synthesized to have a segment composition of 50/50 wt% (Fig. 1).

2.3 Characterization of the copolyester

2.3.1. NMR characterization. ¹H NMR and ¹³C NMR spectra were obtained on a Bruker AMX-300 spectrometer at 25 °C operating at 300.1 MHz (¹H NMR) or 75.5 MHz (¹³C NMR). The copolyester was dissolved in deuterated chloroform (CDCl₃) and the spectra were internally referenced to tetramethylsilane (TMS). Sixty-four scans for ¹H NMR and 1000–10 000 scans for ¹³C NMR were acquired with 32 K and 62 K data points and delay times of 1 and 2 s respectively. Quantitative ¹H NMR spectra were recorded with pulse widths of 6 ms ($\pi/3$) and delay time of 20 s. For ¹³C NMR, the pulse and spectral widths were 4.3 ms ($\pi/2$) and 18 kHz respectively.

2.3.2. Size exclusion chromatography (SEC). The number-average molar mass (M_n) and molar mass distribution (M_w/M_n) values of the novel synthesized copolyester and the same quantities during the degradability studies were determined by SEC (Deltachrom pump, Watrex Comp., autosampler Midas, Spark Instruments, two columns with PL gel MIXED-B LS (10 μ m), separating in the range of molar masses approximately 400–1 \times 10⁷ g mol⁻¹). Tetrahydrofuran (THF) was used as the mobile phase at flow-rate 0.5 mL min⁻¹. The injection-loop volume was 0.1 mL. Measurements were performed with triple viscosity/concentration/light-scattering detection. The set was connected to a light-scattering photometer DAWN DSP-F (Wyatt Technology Corp.) measuring at 18 angles of observation, a modified differential viscometer Viscotek model TDA 301 (without internal light scattering and concentration detectors) and a differential refractometer Shodex RI 71. The data were accumulated and processed using the Astra and triSEC softwares. The evaluation of the triple-detection data is detailed elsewhere.³³

2.4 Preparation of the nanoparticles (NPs)

The polymeric nanoparticles were prepared by using a nanoprecipitation protocol in water and varying the copolymer concentration from 0.25 to 1.00 wt%. The PBS/PBDL copolyester was first completely dissolved in acetone at 40 °C and

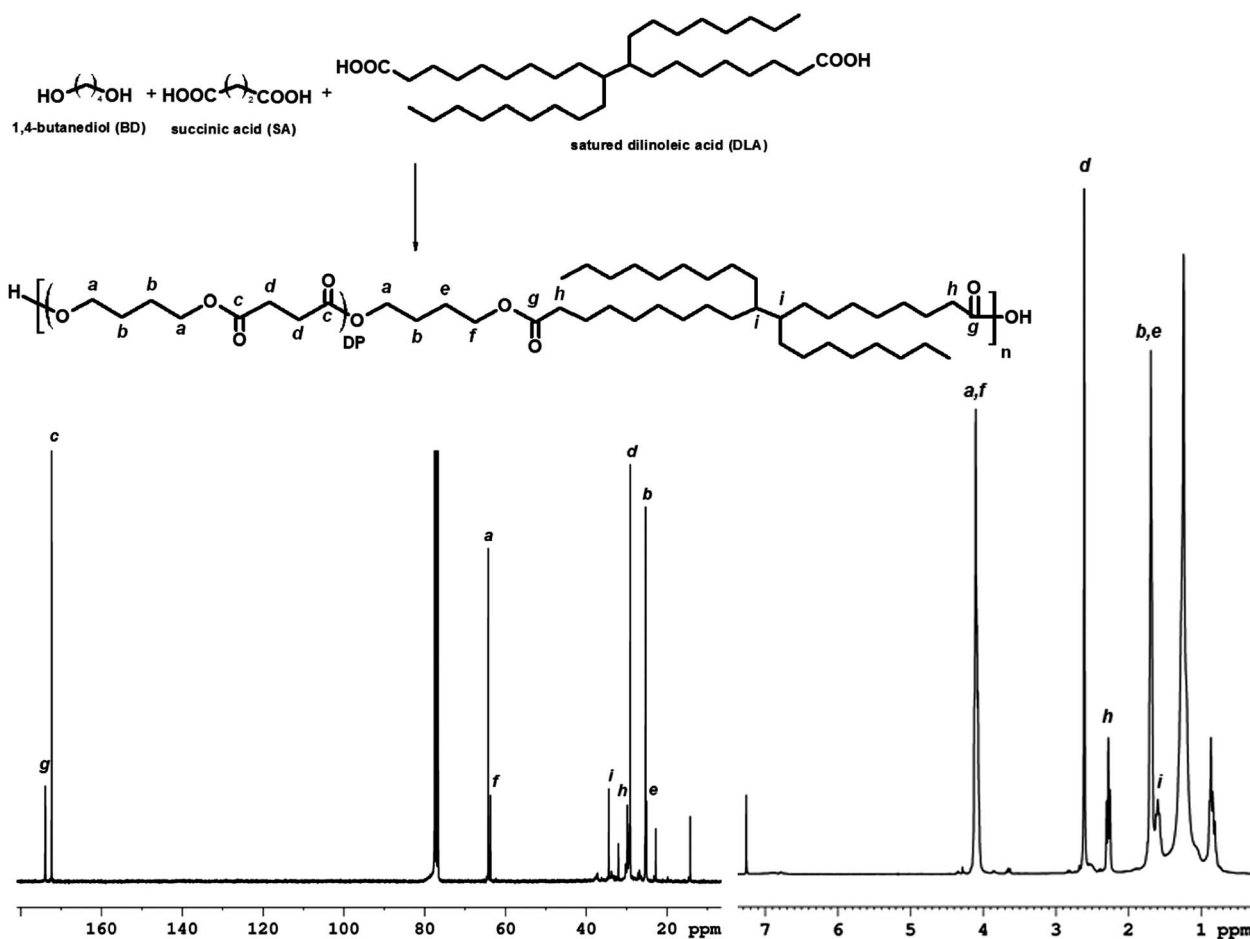


Fig. 1 Structure, ^1H (right) and ^{13}C (left) NMR of the poly(butylene succinate-co-butylene dilinoleate) aliphatic copolyester.

subsequently the organic phase was added drop-wise (EW-74900-00, Cole-Parmer®) to pure water (20 mL) under stirring (Ultra-Turrax T25, IKA, Germany). The organic solvent was further removed by evaporation under reduced pressure at room temperature and the aqueous solution was concentrated to 5 mL. The prepared NPs were used immediately or stored at 4 °C.

2.5 Characterization of the nanoparticles

2.5.1. Dynamic Light Scattering (DLS). The DLS measurements were performed using an ALV CGE laser goniometer consisting of a 22 mW HeNe linear polarized laser operating at a wavelength ($\lambda = 632.8$ nm), an ALV 6010 correlator, and a pair of avalanche photodiodes operating in the pseudo cross-correlation mode. The samples were loaded into 10 mm diameter glass cells and maintained at 25 ± 1 °C. The data were collected using the ALV Correlator Control software and the counting time was 30 s. In order to avoid multiple light scattering, the samples were diluted 100 times before the measurements.³⁴ The measured intensity correlation functions $g_2(t)$ were analyzed using the algorithm REPES (incorporated in the GENDIST program)³⁵ resulting in the distributions of relaxation times shown in equal area representation as $\tau A(\tau)$. The mean relaxation time or relaxation frequency ($\Gamma = \tau^{-1}$) is related to the diffusion coefficient (D) of the nanoparticles as $D = \frac{\Gamma}{q^2}$ where $q = \frac{4\pi n \sin(\theta/2)}{\lambda}$

is the scattering vector being n the refractive index of the solvent and θ the scattering angle. The hydrodynamic radius (R_H) or the distributions of R_H were calculated³⁶ by using the well-known Stokes–Einstein relation:

$$R_H = \frac{k_B T}{6\pi\eta D} \quad (1)$$

where k_B is the Boltzmann constant, T is the absolute temperature and η is the viscosity of the solvent.

2.5.2. Static light scattering (SLS). In the SLS mode, the scattering angle was varied from 30 to 150° with a 10° stepwise increase. The absolute light scattering is related to the weight-averaged molar mass ($M_{w(\text{NP})}$) and to the radius of gyration (R_G) of the nanoparticles by the Zimm formalism represented as:

$$\frac{Kc}{R_\theta} = \frac{1}{M_w} \left(1 + \frac{R_G^2 q^2}{3} \right) \quad (2)$$

where K is the optical constant which includes the square of the refractive index increment (dn/dc), R_θ is the excess normalized scattered intensity (toluene was applied as standard solvent) and c is the polymer concentration given in mg mL^{-1} . The refractive index increment (dn/dc) of the PBS/PBDL NPs in pure water (0.153 mL g^{-1}) was determined using a Brice–Phoenix differential refractometer operating at $\lambda = 632.8$ nm.

2.5.3 Electrophoretic Light Scattering (ELS). The ELS measurements were employed in order to determine the average zeta potential (ζ) of the nanoparticles, which was done using the Zetasizer NanoZS instrument (Malvern Instruments, UK). The equipment measures the electrophoretic mobility (U_E) of the nanoparticles and converts the value to the ζ -potential (mV) through Henry's equation. Henry's function was calculated through the Smoluchowski approximation.

2.5.4. Small Angle X-ray Scattering (SAXS). The SAXS experiments were conducted at the SWING SAXS beamline of the Synchrotron SOLEIL (Gif-sur-Yvette, France). The samples were loaded into sealed borosilicate capillaries (~2 mm diameter). The collimated beam ($\lambda = 1.033 \text{ \AA}$) crossed the samples towards an evacuated flight tube and was scattered to a $17 \text{ cm} \times 17 \text{ cm}$ PCCD-170170 CCD Detector (Aviex). The sample-to-detector distance was chosen in such way that the q -range $0.02\text{--}2.1 \text{ nm}^{-1}$ could be covered. At each measurement, 10 frames of 0.1 s exposure time were collected. They were further normalized by the sample transmission and subsequently averaged and converted to $I(q)$ vs. q profiles using the Foxtrot software. The resulting $I(q)$ vs. q scattering curves were corrected by the subtraction of the scattering of the pure solvent and they could be fitted by using the form factor of homogeneous spheres. The fitting procedures were performed using the SASfit software which makes use the least-squares fitting approach for minimizing the chi squared (χ^2) parameter. The SASfit software package was developed by J. Kohlbrecher.³⁷

2.5.5. Transmission electron microscopy (TEM). The TEM images were recorded using a JEM 200CX (Jeol, Japan) microscope operating at 100 kV and equipped with a digital camera. Brightness, contrast and gamma corrections were performed with standard software. The nanoparticles were diluted 100 times and $5 \mu\text{L}$ of the aqueous solutions were dropped onto a copper TEM grid (300 mesh) coated with carbon film. The TEM images were analyzed using the ImageJ software. The reported particle size and size distribution are the results of the analysis of 150 particles.

2.6 Paclitaxel (PTX) drug loading and loading efficiency

The total amount of the hydrophobic model drug paclitaxel (PTX) loaded into the NPs (total drug feeding subtracted from the free-drug amount collect after the ultrafiltration–centrifugation step described below) was measured by HPLC (Shimadzu, Japan) using a reverse-phase column Chromolith Performance RP-18e ($100 \times 4.6 \text{ mm}$, eluent water–acetonitrile with acetonitrile gradient 0–100 vol%, flow rate = 1.0 mL min^{-1}).

To start, $100 \mu\text{L}$ of the drug-loaded NPs was collected from the bulk sample and diluted to $900 \mu\text{L}$ with acetonitrile. Afterwards, $20 \mu\text{L}$ of the final sample was injected through a sample loop. PTX was detected at 227 nm using ultraviolet (UV) detection. The retention time of PTX was 11.80 min in such experimental conditions. An analytical curve with linear response in the range ($0.5\text{--}100 \mu\text{g mL}^{-1}$) was obtained and used to determined PTX contents. The free-drug was separated from the drug-loaded NPs by ultrafiltration–centrifugation (Ultrafree-MC 10 000 MW, Millipore) as detailed elsewhere.³⁸ The samples were centrifuged

at 6000 rpm for 30 min. The amount of PTX in the nanoparticles was measured in the filtrate after the dissolution of NPs by using acetonitrile as described earlier. The drug-loading content (LC) and the drug-loading efficiency (LE) were calculated by using the following equations:

$$\text{LC (\%)} = \frac{\text{drug amount in nanoparticles}}{\text{mass of nanoparticles}} \times 100 \quad (3)$$

$$\text{LE (\%)} = \frac{\text{drug amount in nanoparticles}}{\text{drug feeding}} \times 100 \quad (4)$$

2.7 Drug release

The release experiments were carried out at $37 \text{ }^\circ\text{C}$ by using water as the release media.³⁹ Aliquots (0.5 mL) of drug-loaded NPs were loaded into 36 Slide-A-Lyzer MINI dialysis microtubes with MWCO 10 kDa (Pierce, Rockford, IL). These microtubes were dialyzed against 3 L of water with gentle stirring. The drug release experiments were performed in triplicate. At each sampling time, three microtubes were removed from the dialysis system and 0.3 mL from each microtube was sampled and diluted to a final volume of 1.0 mL with acetonitrile. The PTX content at each sampling time was then determined *via* HPLC by applying the same procedure previously described. The 0.2 mL remaining in the microtubes was removed and the dimensions of the PTX-loaded NPs were probed by DLS and SLS. The drug diffusion through the membrane was not the rate-limiting step as recently evidenced.⁴⁰

2.8 Biodegradability studies

The biodegradation rate of the PBS/PBDL NPs was followed by SEC. The suspension of nanoparticles (~20 mg of NPs) was loaded in a membrane dialysis bag with MWCO 6–8 kDa (Spectra-Pore®) and then incubated in 0.10 M phosphate buffer solution (PBS) (pH 7.4, $37 \text{ }^\circ\text{C}$). At each sampling time, an aliquot of 2 mL of the incubated NPs was removed and their hydrodynamic dimension probed by DLS. The sample was further lyophilized and analyzed by SEC. All the measurements were done in triplicate.

2.9 Cytotoxicity assays

2.9.1. Mouse splenocytes. The mice (C57B/6, H- 2b; Balb/c, H-2d) were killed by cervical dislocation. The spleens were removed aseptically, stripped of fat and placed in an ice-cold RPMI 1640 culture medium (Sigma, USA) supplemented with 4 mM L-glutamine, 50 mM 2-mercaptoethanol, 1 mM sodium pyruvate, 4.5 g L^{-1} glucose, antibiotics (penicillin/streptomycin, Sigma, USA), and 10% v/v heat-inactivated fetal calf serum (FCS). Cells were grown in cultivation flasks at $37 \text{ }^\circ\text{C}$ with 5% CO_2 . Single-cell suspensions were obtained by gentle homogenization of mouse spleen in a tissue homogenizer. The spleen lymphocytes were separated from the debris and then washed twice (5 min at 800 g at $4 \text{ }^\circ\text{C}$). Red blood cells were lysed with Tris-buffered ammonium chloride solution. Lymphocyte viability was assessed by Trypan Blue exclusion test. The viability of the cells used was >95%. All procedures were approved by the Animal Welfare Committee of the Institute of Microbiology, ASCR, v.v.i.

2.9.2. Proliferation assay of mouse splenocytes. To estimate cell proliferation, [3H]-thymidine incorporation was assessed using a [3H]-thymidine incorporation assay. NUNC/NON 96-well, flat-bottomed plates were seeded with 5×10^4 splenocytes/well. Concentrations of 0.01 to 1.00 mg mL⁻¹ of the NPs were then added to the wells to a final well volume of 200 μ L. The plates were cultured in 5% CO₂ for 48 h at 37 °C. Before the last 6 h of incubation, 18.5 kBq of [3H]-thymidine was added per well. The cells were then collected onto glass fiber filters (Filtermat, Wallac, Finland) using a cell harvester (Tomtec, Orange, CT). After drying, the fibre filter was placed into a sample bag, a solid scintillator (MeltiLex, Wallac) was applied and the bags were sealed (Microsealer, Wallac). Counting was performed in a 1450 MicroBeta Trilux (Wallac). Cells cultivated in fresh medium were used as control. The results were calculated as the arithmetic mean of the c.p.m. in four individual wells. Data represent cell number in relation with the control standard deviation was lower than 15%. The stimulation index (SI) was calculated by the following formula:

$$SI = \frac{\text{mean cpm in cell cultures}}{\text{mean cpm in control cultures}} \quad (5)$$

3. Results and discussion

3.1 Characterization of the PBS/PBDL copolyester

The synthetic strategies were already fully detailed elsewhere.²⁸ The structure of the synthesized poly(butylene succinate-co-butylene dilinoleate) PBS/PBDL copolyester is portrayed in Fig. 1 and its characteristics are given in Table 1.

The number-average molar mass (M_n) of the copolyester was estimated by SEC as 35×10^3 g mol⁻¹ and it holds a reasonable degree of polydispersity ($M_w/M_n = 1.88$). The composition of the copolyester was determined from ¹H and ¹³C NMR (Fig. 1). In ¹H NMR the methylene protons of the BD segments appear at 1.69 (*b, e*) and 4.1 ppm (*a, f*). The signals at 2.61 ppm (*d*) are due to the methylene protons of the SA segment. Methylene protons of the DLA segment adjacent to the ester bond appear as the duplet at 2.27 ppm (*h*) and the protons of the tertiary carbon appear at 1.59 ppm (*i*). The remaining protons at 7.23, 1.24 and 0.87 ppm are related respectively to the hydroxyl groups of the copolyester and to the ethyl and methyl carbon chains of DLA. The ¹³C NMR spectra signals of BD in the PBS segment appear at 25.3 ppm (*b*) and 64.2 ppm (*a*). These signals are shifted to 25.0 ppm (*e*) and 63.7 ppm (*f*) in the PBDL segment. Additionally, the carbonyl signal of SA in the PBS segment and the carbonyl signal of the DLA segment shifted to 172.3 ppm (*c*) and 173.9 ppm (*g*) respectively, suggesting a complete polycondensation reaction. The molar composition of the copolyester was determined using the relative

integrals of SA arising from PBS (*d* or *c*) and the dimerized fatty acid from PBDL (*h* or *g*). The ratio composition was calculated as 3 : 1 (PBS : PBDL) which is close to the feeding monomer ratio (3.6 : 1 for 50/50 wt%). Characteristic signals of the “couplings” in ¹H-NMR and ¹³C-NMR spectra were not found, meaning that the resulting copolymer exhibits a statistical distribution of monomer units. This was confirmed by ¹³C NMR spectra, which describes the division of the carbonyl groups (C=O) in the copolymer, area ~ 64 ppm. Both signals of carbonyl groups correspond to the ratio 1 : 3 confirming statistical distribution of monomer units (Fig. S1, ESI†).

The nanoprecipitation protocol requires an organic solvent in which the PBS/PBDL is fully soluble. The solvent must be also miscible in water and it must have a low boiling point to allow further easy evaporation. Among the standard solvents, the best choice was acetone. The distribution of sizes of the dissolved PBS/PBDL copolyester in acetone was assessed by DLS and it is given in Fig. 2.

The size distribution of PBS/PBDL in acetone suggests the presence of diffusing scattering objects having hydrodynamic radius $R_H = 9.5$ nm and it is certainly related to the presence of single dissolved PBS/PBDL copolyester chains in acetone.

3.2 Characterization of the nanoparticles

The nanocarriers were prepared by means of nanoprecipitation. The PBS/PBDL copolymer is insoluble in water and it is expected to undergo precipitation after the diffusion of the solvent (acetone) into the aqueous phase leading to the formation of well-defined nanoparticles. Primarily, the size, size distribution and the stability of the nanoparticles were investigated. It is worth mentioning that all nanoparticles prepared were

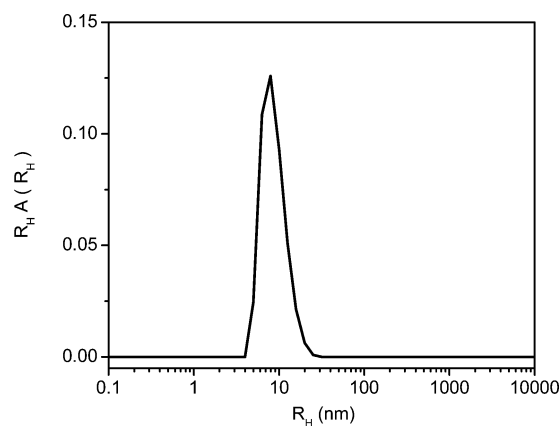


Fig. 2 R_H distribution for PBS/PBDL dissolved in acetone at 5 mg mL⁻¹ (40 °C).

Table 1 Characteristics of the synthesized PBS/PBDL copolyester

PBS (wt%) ^a	PBDL (wt%) ^b	DP ^a	$M_n/10^3$ g mol ^{-1b}	M_w/M_n^b	$T_g/^\circ\text{C}$	$d/\text{g mL}^{-1c}$
50.0	50.0	3	35.0	1.88	-61.0	1.08

^a Composition and degree of polycondensation estimated by NMR. ^b Measured by SEC. ^c Density measured by flotation in aqueous zinc chloride solution.

macroscopically homogeneous and they showed good macroscopic temporal stability over months. The nanoparticles were probed by dynamic light scattering and the results are given in Fig. 3.

The autocorrelation functions measured at 90° and the respective normalized distributions of relaxation times $\tau A(\tau)$ for different starting polymer concentrations are given in Fig. 3a. The diffusive behavior of the investigated nanoparticles was confirmed by the linear q^2 dependence of the decay rate. Therefore, the Stokes–Einstein equation could be used to determine hydrodynamic radii (R_H) of the assembled objects (Table 2). The existence of a narrow, unimodal particle size distribution with an increase in size as a function of the starting polymer concentration was detected. This tendency is clearly observed by looking at Fig. 3b where the higher the starting polymer concentration the lower is the slope of the linear profiles that quantitatively gives the diffusion coefficient of the NPs, which is finally inversely proportional to their hydrodynamic radius (eqn (1)).

The size of the NPs ranges from 34.5 to 56.7 nm (*i.e.* mean diameters from 69.0 to 113.4 nm). By taking into account that the NPs are produced in a large amount of the nonsolvent water, the increase in nanoparticle size as a function of the polymer concentration might be explained by the nucleation-aggregation

mechanism.⁴¹ Therefore, when the solution is sufficiently saturated, critical nuclei of pure solute are formed and they grow by capturing solute molecules from the surroundings. The increase in the number of available copolymer chains (higher concentration) leads to an increase in the number of nuclei and consequently in the probability of nuclei encounters. Each encounter causes aggregation of nuclei thereby increasing the nanoparticle size (and the molar mass of the nanoparticles $M_{w(NP)}$) when nanoprecipitation occurs (Table 2).

The formation of spherical nanoparticles was confirmed by transmission electron microscopy (TEM) and is shown in Fig. 4 (inset). The size distribution histogram resulting from the image analysis is given in the ESI† (Fig. S2). The number-average mean diameter (D_N) and the polydispersity index ($P_{TEM} = D_w/D_N$) were determined as detailed elsewhere⁴² and were equal to 72.4 nm and 1.12, respectively ($c_{polymer} = 5.0 \text{ mg mL}^{-1}$). This confirms the relatively narrow size distribution of the NPs, although the determined mean size from the TEM image analysis is evidently smaller than the determined by DLS. This is in part due to dehydration of the entities caused by solvent evaporation under the high vacuum conditions employed during TEM imaging. However, discrepancies are also expected because DLS reports an intensity-average dimension whereas TEM reports a number-average dimension. Therefore, TEM images generally undersize relative to DLS data. SAXS measurements were also performed to probe the size, shape and dispersity of the nanoparticles. Fig. 4 shows the SAXS profile of the PBS/PBDL nanoparticles for the polymer concentration 5.0 mg mL^{-1} as the representative example.

In widely separated systems (as in the current case), $I(q)$ is due to the form factor $P(q)$ of the scattering objects. Herein $P(q)$ was modelled geometrically as homogenous spheres:

$$I(q) = V_p^2 \Delta\sigma^2 P(q, R) = \left(\frac{4}{3}\pi R^3 \Delta\sigma\right)^2 \left(\frac{3[\sin(qR) - qR \cos(qR)]}{(qR)^3}\right)^2 \quad (6)$$

The sample polydispersity was considered using the log-normal distribution for which the probability density function is given by:

$$f(R, \mu, \delta) = \frac{1}{\sqrt{2\pi}\delta R} \exp\left(-\frac{\ln(R/\mu)^2}{2\delta^2}\right) \quad (7)$$

where R is the average radius, μ is the location parameter and δ^2 is the variance. The parameter δ is the standard deviation which gives the quantitative information about the width of the distribution. This fitting approach described the experimental results reasonably well and led to values of $D = 2R = 79.8 \text{ nm}$ and $\delta = 0.144$. It is also worth noting that the high quality of the fitting, particularly at the low- q range of the SAXS profile, hints at the absence of aggregating nanoparticles due their electrostatic stabilization as hereafter discussed. The size of the nanoparticles is within the optimal range for injectable drug release and drug delivery systems where the particle size should be smaller than 200 nm .^{43,44} Another requirement for drug delivery nanoparticles which plays an important role in colloidal stability and later in controlled drug release is the narrow size distribution. The nanoparticle distribution width calculated by the cumulant

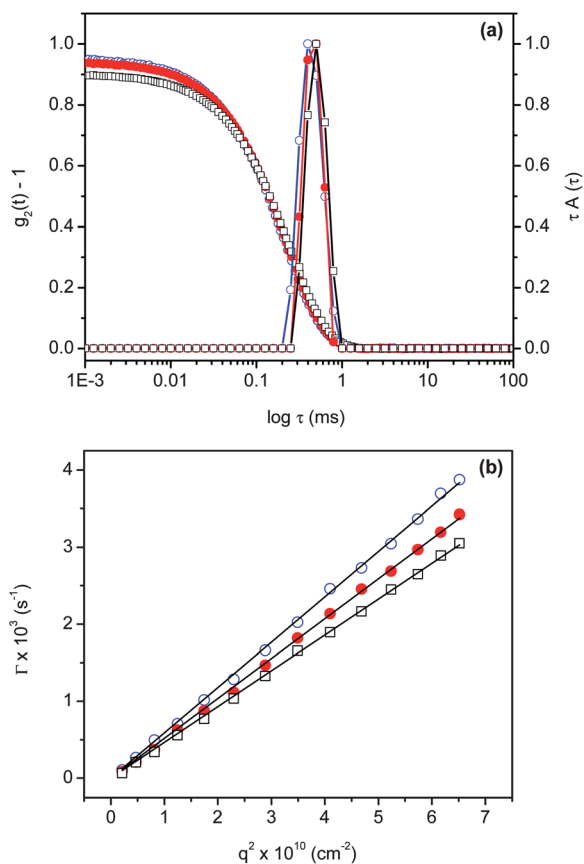


Fig. 3 (a) Autocorrelation functions $g_2(t) - 1$ measured at scattering angle 90° and the respective distributions of the relaxation times $\tau A(\tau)$ revealed by REPES analysis for PBS/PBDL nanoparticles at starting polymer concentrations 2.5 mg mL^{-1} (○), 5.0 mg mL^{-1} (●) and 10 mg mL^{-1} (□). (b) Angular variation of the frequency $\Gamma = 1/\tau$ as a function of q^2 .

Table 2 Physico-chemical characteristics of the produced PBS/PBDL nanoparticles

Entry	$c_{\text{polymer}}/\text{mg mL}^{-1}$	R_{H}/nm	R_{G}/nm	$R_{\text{G}}/R_{\text{H}}$	$M_{\text{w(NP)}}/10^8 \text{ g mol}^{-1}$	$d/\text{g mL}^{-1}$	Dispersity	ζ/mV
NP1	2.5	34.5	40.5	1.17	0.78	0.38	0.067	-36.0
NP2	5.0	46.7	52.6	1.13	1.03	0.39	0.083	-37.0
NP3	10.0	56.7	59.0	1.04	1.74	0.35	0.094	-35.0

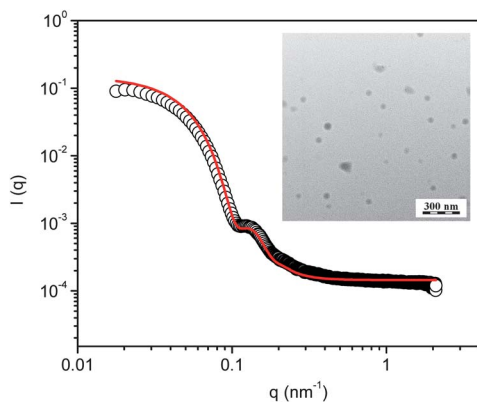


Fig. 4 SAXS data (circles) and corresponding curve fitting (line) for PBS/PBDL nanoparticles produced from starting polymer concentration $c_{\text{polymer}} = 5.0 \text{ mg mL}^{-1}$. The inset portrays the TEM image in the same conditions.

analysis⁴⁵ ranges from 0.067 to 0.094 (Table 2, dispersity). These values are even lower than the values found in similar nanoparticulate systems using surfactants.^{29,46,47}

The partial Zimm plot results are reported in Fig. 5 and Table 2. The dn/dc value of the copolyester nanoparticles in water was found to be equal to 0.153 mL g^{-1} . The values of the molar mass of the nanoparticles ($M_{\text{w(NP)}}$) and their radius of gyration (R_{G}) were estimated from the slope of the curves and from the inverse of the intercepts in Fig. 5 (eqn (2)). The concentration of polymeric nanoparticles was preset to 0.1 mg mL^{-1} . The full Zimm plot of NP3 ($c_{\text{polymer}} = 10.0 \text{ mg mL}^{-1}$) is given in the ESI†

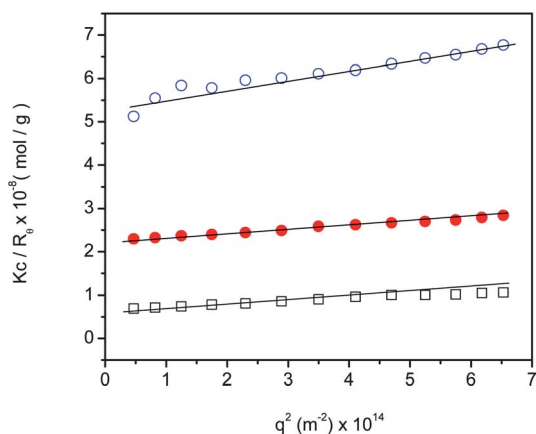


Fig. 5 Static light scattering (Kc/R_0 vs. q^2) for PBS/PBDL nanoparticles prepared starting at 2.5 mg mL^{-1} (○), 5.0 mg mL^{-1} (●) and 10 mg mL^{-1} (□) polymer concentrations. The concentration of polymeric nanoparticles in all the samples was fixed at 0.1 mg mL^{-1} .

(Figure S3). The very similar results allow the use of the partial Zimm plot version.

The $M_{\text{w(NP)}}$ increases as a function of the copolymer concentration for the reasons aforementioned. The static and hydrodynamic dimensions of a scattering object are functions of the macromolecular structure and the combination of both provides qualitative information about its architecture. It is well established that the ratio $\rho = R_{\text{G}}/R_{\text{H}}$ is a characteristic parameter related to the conformation of polymer chains and self-assembled macromolecular objects in solution. For hard-spheres, random coils and rod-like structures ρ -values of 0.775, 1.78, and ≥ 2 have been reported.⁴⁸ Furthermore, the ρ -value of spherical objects is dependent on the inner structure and compactness,⁴⁹ being close to 0.775 for very compact spheres, $\rho \sim 0.8\text{--}0.9$ for block copolymer micelles due to solvation phenomena⁵⁰ and $\rho \sim 1.0$ for hollow spheres and vesicles. Moreover, $R_{\text{G}}/R_{\text{H}}$ for spherical nanoparticles made from regular branched polymers or statistical randomly polycondensates are found to be within 0.977–1.127.^{51–53} These values were found for polymeric nanoparticles following the soft sphere model.^{48,51} The $R_{\text{G}}/R_{\text{H}}$ ratios of the PBS/PBDL nanoparticles at different copolymer concentrations (Table 2) are found to be in the same range suggesting that the nanoparticles are not compact. Similar ratios from 1.06 to 1.2 and density lower than 0.01 g mL^{-1} were found for poly(sebacic anhydride)-*co*-polyanhydride nanoparticles prepared by using the nanoprecipitation protocol.^{54,55} The authors suggested that the results are related to the hyperbranched structure of the nanoparticles and to high amounts of water entrapped inside the assemblies. The average density (d) of the investigated nanoparticles was calculated by using the determined values of $M_{\text{w(NP)}}$ and R_{H} as:⁵⁶

$$d = \frac{3M_{\text{w(NP)}}}{4\pi N_{\text{A}}(R_{\text{H}})^3} \quad (8)$$

wherein N_{A} is the Avogadro constant. The d -values are independent of the copolymer concentration and at about 0.37 g mL^{-1} (Table 2). The density of the nanoparticles is reasonably low, suggesting that they are porous and probably water-swollen. This is also suggested by the calculated ρ -values characteristic of soft spherical nanoparticles. The soft behavior linked to the water entrapment can explain the remarkable particle stability without the addition of stabilizers (surfactants). The entrapped water inside the particles reduces their density and hydrophobicity and simultaneously increases the particle charge, as is revealed by the ζ -potential measurements (Table 2). The negative ζ -potentials were attributed to the presence of negative charges in the oxygen of the carbonyl group in the ester bounds and to the remaining carboxyl terminal groups in the multiblock copolymer nanoparticles.^{48,57} The entrapped water should increase electron

delocalization in the oxygen of the carbonyl group in the ester bounds and increase the particle charge and consequently their stability.

3.3 Drug-loading and loading efficiency

The loading content (LC) is the drug-loading capacity of a nanocarrier and it is related to its mass (eqn (3)) whereas LE is the drug-loading efficiency and it is related to the total drug feeding (eqn (4)). Ideally, a successful nanoparticulate system should have a high drug-loading capacity thereby reducing the quantity of matrix material for administration and a high loading-efficiency to avoid drug losses and therapy commitment. Drug loading and entrapment efficiency are strongly dependent on the solid-state drug solubility in the polymer matrix^{29,58} which is dependent on the polymer composition, molar mass, polymer–drug interactions and the presence of terminal functional groups (ester or carboxyl).⁵⁹ To investigate the LC and LE of the PBS/PBDL nanocarriers, PTX was used as the hydrophobic drug model and loaded to the novel copolyester NPs. The drug-loaded NPs were prepared using essentially the same procedure previously described except that in such a case a known amount of PTX was dissolved in acetone along with the PBS/PBDL copolyester. The LC of the PBS/PBDL NPs was investigated in the range 1–10% $w_{\text{drug}}/w_{\text{polymer}}$. It has been found that the stability of the drug-loaded PBS/PBDL NPs was limited to $\sim 6\text{--}7\%$ $w_{\text{drug}}/w_{\text{polymer}}$ drug feeding. For comparison, two well-known FDA-approved polyesters (PLGA and PLA) were also used to prepare PTX-loading NPs. PBS/PBDL, PLGA and PLA PTX-loaded NPs were prepared at 2.5% $w_{\text{drug}}/w_{\text{polymer}}$ drug feeding. In such conditions, the LC of the PBS/PBDL NPs was $\sim 2.5\%$ $w_{\text{drug}}/w_{\text{polymer}}$ and LE $\sim 100\%$. On the other hand, the PXT LC was $\sim 0.90\%$ $w_{\text{drug}}/w_{\text{polymer}}$ and LE $\sim 89\%$ for PLGA NPs and for PLA NPs the LC and LE were significantly lower $\sim 0.73\%$ and $\sim 70\%$ respectively. These results show that the novel synthesized polyester exhibits higher entrapment efficiency and drug loading capacity compared to PLA or PLGA suggesting stronger hydrophobic interactions between the PBS/PBDL copolyester matrix and the PTX drug. Accordingly, PBS/PBDL copolyester nanoparticles seem to be a promising alternative to hydrophobic drug encapsulation in biomedical and drug delivery applications.

3.4 Drug release experiments

Generally, the drug release is governed by two different mechanisms: *i*) a standard diffusion-controlled release or *ii*) a triggered pathway initiated by changing the environmental conditions such as pH or temperature. Additionally, considering nanoparticles produced from biodegradable polymers, the drug release is also supposed to be controlled by the bulk erosion rate.³⁹ It is well-known that the drug diffusion-controlled release depends on its effective diffusion coefficient throughout the polymer matrix, which in turn depends on its porosity and tortuosity.^{29,58} As mentioned above, the stability of the drug-loaded PBS/PBDL NPs is limited to $\sim 6\text{--}7\%$ $w_{\text{drug}}/w_{\text{polymer}}$ drug feeding. Accordingly, the release experiments were carried out by setting the loading content at $\text{LC} = 5.0\%$ $w_{\text{drug}}/w_{\text{polymer}}$. The LE was reasonably reproducible and nearly constant at $\sim 95\%$ and

the drug release was monitored by HPLC and light scattering (DLS and SLS). The results are shown in Fig. 6.

The release experiments indicate that approximately 40% of the encapsulated PTX is released within the first 12 h whilst only 10% is sustained in the polymeric core after 120 h (Fig. 6a). The slow pharmacokinetic release might be attributed to the hydrophobicity of the manufactured PBS/PBDL nanocarriers and to the poor water solubility ($\sim 0.3 \mu\text{g mL}^{-1}$) of the entrapped drug. In the current case, certainly the drug release is controlled by the

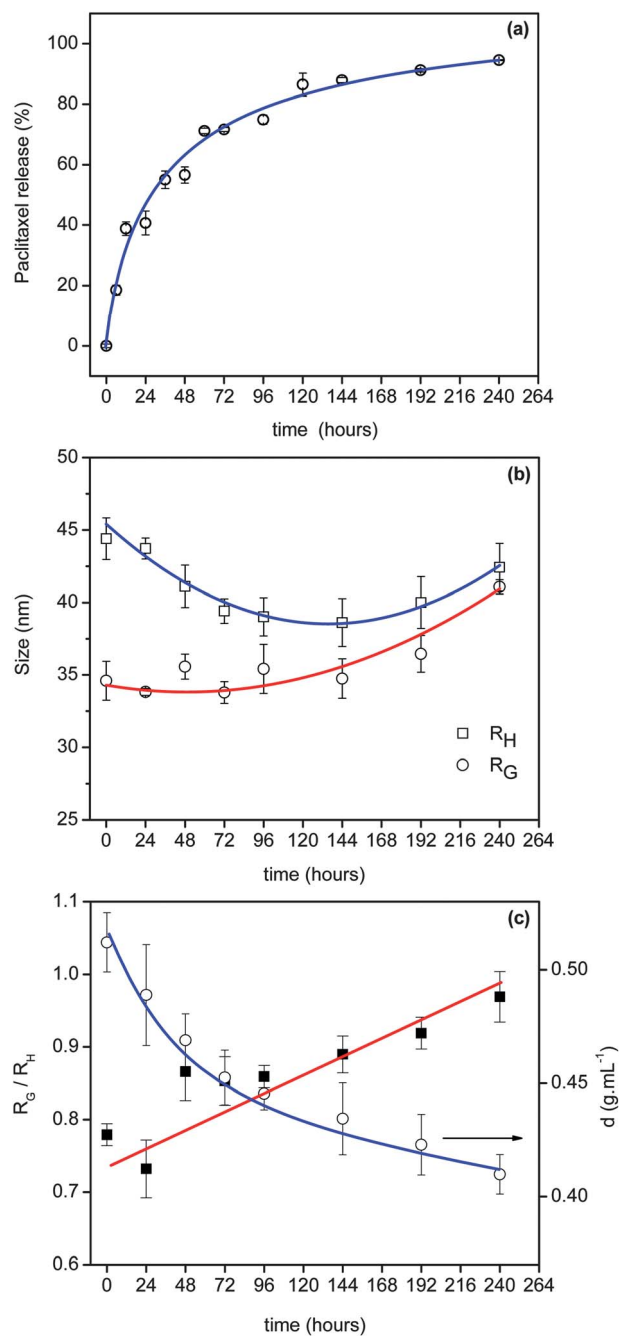


Fig. 6 Drug release profile from PTX-loaded PBS/PBDL NPs prepared using $c_{\text{polymer}} = 5.0 \text{ mg mL}^{-1}$ (a). R_G and R_H (b) and R_G/R_H and nano-particle density (c) vs. time during PTX release.

diffusion of the drug through the polymer matrix and by the hydrolysis of the PBS/PBDL copolymer.

As previously mentioned, the combination of SLS and DLS measurements is appropriate to measure hydrodynamic dimensions of nanoparticles and it might also provide informations on the shape and inner structure of the scattering objects. Furthermore, quantitative information on the density of the nanoparticles and draining properties might be further probed.⁴⁸ The drug encapsulation and release was also followed by DLS and SLS measurements and the data in Fig. 6b clearly indicate that the drug encapsulation reduces the dimensions of the nano-carriers. By comparing with the dimensions of the drug-free NPs (Table 2, $c_{\text{polymer}} = 5.0 \text{ mg mL}^{-1}$), the hydrodynamic dimension (R_{H}) was reduced from 46.7 (drug-free) to 44.0 nm (drug-loaded at $t = 0 \text{ h}$) whereas their radius of gyration (R_{G}) has been reduced from 52.6 (drug-free) to 35.0 nm (drug-loaded at $t = 0 \text{ h}$).

The reduction in R_{G} is more pronounced than the reduction in R_{H} and it consequently reflects the reduction on the ρ -value from 1.13 (drug-free) to 0.79 (drug-loaded at $t = 0 \text{ h}$). Simultaneously, the density of the particles increases from 0.39 g mL^{-1} to 0.51 g mL^{-1} . These experimental data certainly reflect the softness of the NPs⁶⁰ and the transition of the inner structure from a water-swollen condition (drug-free NPs) towards a higher degree of compactness (drug-loaded NPs). The PTX encapsulation led to a higher degree of compactness once the ρ -value was displaced towards the hard-sphere character. Indeed, the stability of the drug-free PBS/PBDL nanoparticles in pure water suggests that they are partially drained or that the polymer chains forming the NPs are not fully collapsed. The values of their density ($\sim 0.37 \text{ g mL}^{-1}$) are much lower than the density of the bulk copolymer (1.08 g mL^{-1}) pointing out that the polymer chains forming the NPs are loosely packed and therefore, they must certainly be swollen by water. The PBS/PBDL copolyester comprises a less hydrophobic segment (PBS) containing numerous ester bonds. Accordingly, it is reasonable to accept the water-swollen characteristic of the NPs in the drug-free conditions. As matter of fact, PLA nanoparticles (which are hydrophobic) are generally highly swollen by water ($d \sim 0.15 \text{ g mL}^{-1}$), which confers them considerable stability.⁶¹

The swelling-collapse transition of the polymeric nanoparticles caused by the hydrophobic drug loading is unmistakably supported by the SAXS data (Fig. 7). The SAXS data of the unloaded and PTX-loaded NPs were fitted with the form factor of homogeneous spheres. The electron density of PBS/PBDL was calculated by using the average chemical composition of the copolyester and its density as being equal to $0.353 \text{ e}^{-} \text{ \AA}^{-3}$. The electron density of water ($0.334 \text{ e}^{-} \text{ \AA}^{-3}$) is incidentally close to the one calculated for the copolyester. Consequently, contrast changes are hardly seen in the swelling-collapse evolution. Nevertheless, the reduction in the dimension of the NPs caused by drug-loading is clearly evidenced by the displacement of the bump at $q \sim 0.15 \text{ nm}^{-1}$ towards the high- q range. The average radius (R) of the NPs is reduced from 39.9 to 35.2 nm by the addition of 5.0% $w_{\text{drug}}/w_{\text{polymer}}$ of the hydrophobic guest molecule. It suggests that PTX is entrapped inside the copolyester matrix during the drug encapsulation resulting in the shrinking of the nanoparticles caused by water draining. The less hydrophobic segment of the copolyester (PBS) is supposed to be responsible for a thick stabilizing layer and the NPs packing is

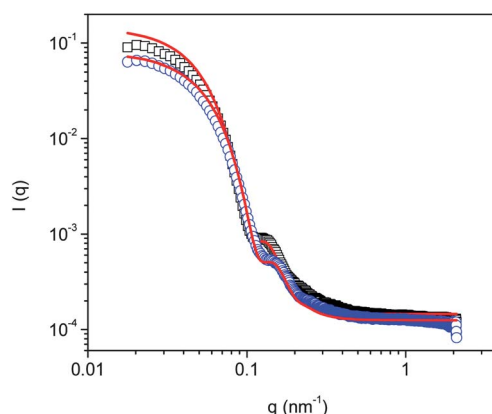


Fig. 7 SAXS data (circles) and corresponding curve fitting (line) for unloaded (\square) and 5.0% $w_{\text{drug}}/w_{\text{polymer}}$ PTX-loaded (\circ) PBS/PBDL nanoparticles produced from starting polymer concentration $c_{\text{polymer}} = 5.0 \text{ mg mL}^{-1}$.

mostly due to the strong hydrophobic interactions expected between the model drug and the highly hydrophobic PBDL segment.

The speculated swelling-collapse transition is schematically represented in Fig. 8.

The drug release is accompanied by a continuous increase of $R_{\text{G}}/R_{\text{H}}$ simultaneous to a continuous reduction in the density of the nanoparticles (Fig. 6c). The R_{G} of the nanoparticles remained nearly constant whereas R_{H} reduces within the first 96 h followed by a slightly increase after 144 h, suggesting diffusion release of the entrapped drug. The initial R_{H} reduction should be related to the PTX diffusion from the PBS/PBDL NPs core towards their surface. This drug-diffusion evolution is linked to simultaneous changes in the inner structure of the NPs. The amount of water remaining in the outer shell of the nanoparticles might be drained out due to the PTX diffusion from the core towards the aqueous media. This leads to an increase in the hydrophobicity along the nanoparticles and to the shrinking of the copolyester matrix as experimentally evidenced by the reduction of the hydrodynamic dimension of the NPs within the first 96 h when PTX diffusion and water draining towards the aqueous media is faster than water draining towards the core. At the end of the PTX release (240 h, 100% PTX released) the R_{G} increases, approaching the initial value (Fig. 6b) and the density of the particles decreases to

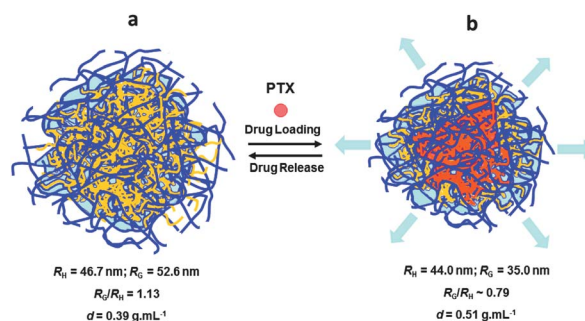


Fig. 8 Schematic representation of the PTX-loading effect. Unloaded (a) and PTX-loaded PBS/PBDL NPs (b). The PTX drug is represented as filled circles and the islands of water are represented in blue.

0.41 g mL⁻¹ (Fig. 6c). The experimental results clearly suggest that when the hydrophobic PTX is totally released, the nanoparticles acquire the initial soft characteristic once the inner core is again water-swollen due to the reduction in its hydrophobicity caused by the drug release. These results point out that the PTX release from PBS/PBDL NPs is mainly governed by drug diffusion and water draining through the polymer matrix. To the best of our knowledge, the combined DLS and SLS measurements used to study structural changes of polymeric nanoparticles induced by the hydrophobic drug encapsulation and drug release have no precedent in the literature. Therefore, these preliminary results demonstrate the feasibility of combined DLS and SLS as a powerful tool to investigate the correlations between the drug release profile and the structure of soft and porous polymeric nanocarriers.

3.5 Degradation behavior of the novel copolyester nanoparticles

The potential biomedical application of hydrophobic biodegradable polymers requires the knowledge of their biodegradation rates. Although PLA, PCL and PLGA are FDA-approved biocompatible and biodegradable polymers, their slow degradation rates limits the polymer concentration threshold for injectable drug release systems. Water-insoluble biodegradable polymers can be degraded by bulk erosion, surface erosion or both simultaneously.³⁹ The degradation mechanism depends on the diffusivity of water inside the polymeric matrix, susceptibility to hydrolysis of the functional groups, and the matrix dimensions. Considering polymeric nanoparticles, as in the current case, water diffusion within the nanoparticles should be faster than bond hydrolysis and therefore, the prevailing eroding mechanism will probably involve bulk degradation.⁶²

The biodegradation rate of the PBS/PBDL copolyester was followed by SEC (by monitoring its molar mass over time) as shown in Fig. 9.

The PBS/PBDL copolyester has an initial weight-average molar mass $M_w = 66 \times 10^3 \text{ g mol}^{-1}$ and as expected, it continuously decreases as a function of time. A pronounced reduction in M_w can be observed in the second week whereas only slight changes were observed in the hydrodynamic dimension of the polymeric nanoparticles. At the end of the second week, precipitates could be observed by the naked eye in the dialysis bag and at the end of the third week, the nanoparticles collapsed and only large ill-defined aggregates were detected by light scattering. In Fig. 9c one can observe that as the degradation progresses, the SEC peak curves shifts towards longer elution time. The initial main peak is essentially decomposed into two smaller peaks indicating the formation of lower molecular weight macromolecules and broadening molar mass distribution due to hydrolytic cleavage of ester bonds. This degradation behavior is strictly connected to the structure of the nanoparticles. As previously mentioned, the PBS/PBDL NPs have a soft characteristic and density equal to 0.37 g mL⁻¹ meaning that they contain a substantial amount of water inside which probably accelerate the hydrolysis process. This is supported by the fast copolyester degradation after two weeks although without a clear reduction in the hydrodynamic dimension of the biodegradable nanoparticles.

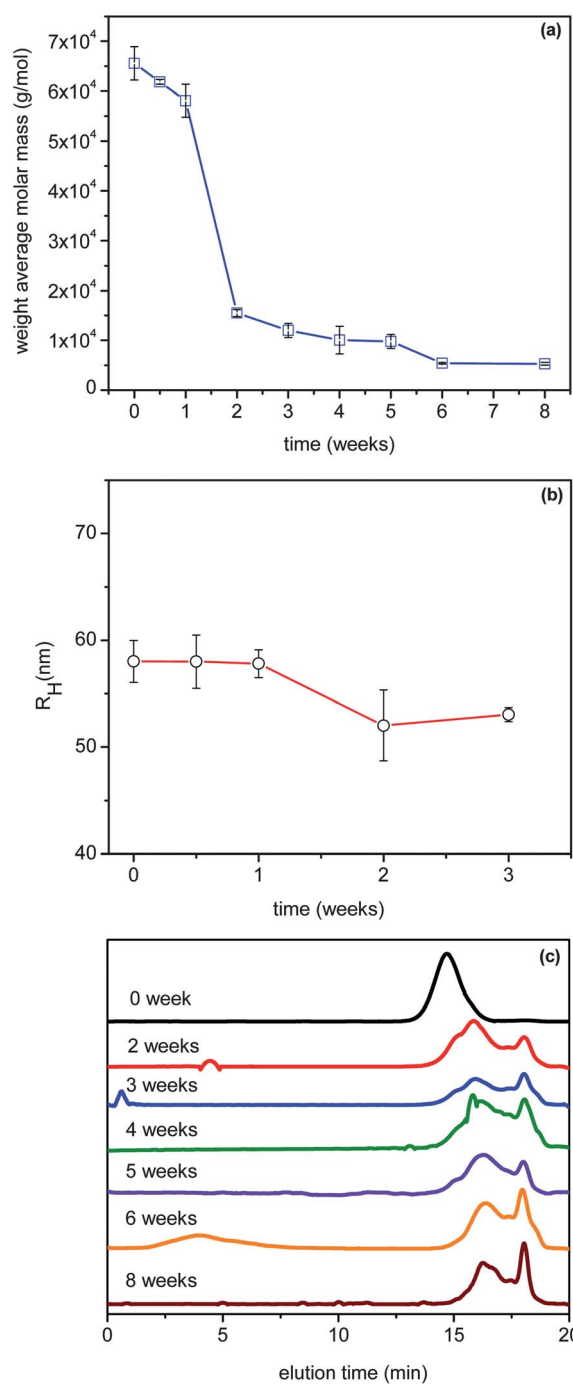


Fig. 9 Weight-average molar mass (M_w) of polymers fragments (a) and hydrodynamic radius (R_H) of the nanoparticles (b) as a function of time during incubation in PBS (pH 7.4). Respective SEC profiles (c).

3.6 Cytotoxicity

The *in vitro* cell proliferation was determined by [3H]-thymidine incorporation into mice C57B/6 and Balb/c unstimulated (spontaneously proliferating) splenocytes incubated with PBS/PBDL NPs, and was used to evaluate the toxicity of the NPs. The results (Fig. 10) show a significant increase in cell proliferation for NPs incubated with both types of mice splenocytes cells in all concentrations evaluated.

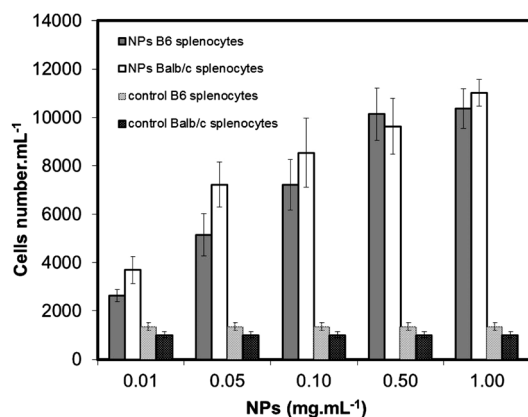


Fig. 10 *In vitro* effect of PBS/PBDL NPs (mg mL⁻¹) on mice Balb/c and B6 splenocytes cell proliferation.

Similar increases in cell proliferation with an increase in the concentration of NPs were also observed on surfactant-containing systems at low surfactant concentrations.⁶³ Surfactant concentrations higher than 0.1–0.5 mg mL⁻¹ disrupt the physiological membranes and become highly toxic to cells. For the current case, surprisingly, the enhanced cell proliferation was observed also at higher NPs concentration. These imply that the investigated PBS/PBDL NPs should be non-toxic in contact with the living systems. This fulfils the basic requirement of good biocompatibility, which is a prerequisite for the biomedical applications.

4. Conclusion

Novel biocompatible and biodegradable PBS/PBDL nanoparticles were produced from aliphatic based monomers consisting of succinic acid, butanediol and dilinoleic acid and their potential applicability in the biomedical field was evaluated. The NPs were prepared by dissolving the PBS/PBDL copolyester in acetone followed by the single-step nanoprecipitation protocol in pure water. TEM and SAXS measurements indicated the spherical shape of the PBS/PBDL NPs. The DLS measurements confirmed the formation of narrowly distributed nanosized particles ($R_H < 60$ nm) suggesting optimized conditions for drug delivery systems. The structure sensitive parameter of the nanoparticles ($\rho = R_G/R_H$) and their density determined by combined DLS and SLS measurements suggested that they are soft and probably composed of a water-swollen core that confers a non-compact character. The water entrapped in the NPs seems to play a crucial role in the particle's stability and in their relatively fast degradation. The polymeric nanoparticles could be loaded with the poorly water-soluble anti-cancer drug paclitaxel (PTX) with encapsulation efficiency $\sim 95\%$ and drug loading content $\sim 6\text{--}7\%$ $w_{\text{drug}}/w_{\text{polymer}}$. The drug encapsulation and release was followed by HPLC and light scattering measurements (DLS and SLS). The drug encapsulation and release were found to modify the inner structure of the nanoparticles and the mechanism is controlled by both water draining and drug diffusion through the polymer matrix. The drug encapsulation leads to shrinking and to a higher degree of compactness of the NPs due to hydrophobic interactions between the polymeric core

and the anticancer drug. The system returns to its initial character as the drug release proceeds. The cell viability experiments demonstrated that the nanoparticles are biocompatible and non-toxic, making them potentially useful for applications in nanomedicine.

Acknowledgements

This work has been sponsored by the Grant Agency of the Czech Republic (Grants IAAX00500803 and P208/10/1600). F. C. G acknowledges financial support from FAPESP (Grant 2010/06348-0). A. Kozłowska and M. El Fray acknowledge financial support from the Polish Ministry of Science and Higher Education (Project N° N209 216538). The authors are grateful to SOLEIL (proposal SWING 20110302) for provision of SAXS beamtime and to S. Meneau and M. Šlouf for assistance during SAXS and TEM measurements respectively. Dr Zdeněk Tuzar is acknowledged for helpful discussions.

References

- M. E. Davis, J. E. Zuckerman, C. H. J. Choi, D. Seligson, A. Tolcher, C. A. Alabi, Y. Yen, J. D. Heidel and A. Ribas, *Nature*, 2010, **464**, 1067–1071.
- D. Peer, J. M. Karp, S. Hong, O. C. Farokhzad, R. Margalit and R. Langer, *Nat. Nanotechnol.*, 2007, **2**, 751–760.
- L. Y. T. Chou, K. Ming and W. C. W. Chan, *Chem. Soc. Rev.*, 2011, **40**, 233–245.
- C.-A. J. Lin, R. A. Sperling, J. K. Li, T.-Y. Yang, P.-Y. Li, M. Zanella, W. H. Chang and W. J. Parak, *Small*, 2008, **4**, 334–341.
- L. E. Euliss, J. A. DuPont, S. Gratton and J. DeSimone, *Chem. Soc. Rev.*, 2006, **35**, 1095–1104.
- A. Kumari, S. K. Yadav and S. C. Yadav, *Colloids Surf., B*, 2010, **75**, 1–18.
- M. Goldberg, R. Langer and X. Q. Jia, *J. Biomater. Sci., Polym. Ed.*, 2007, **18**, 241–268.
- C. S. Ha and J. A. Gardella Jr., *Chem. Rev.*, 2005, **105**, 4205–4232.
- S. Schubert, J. T. Delaney Jr. and U. S. Schubert, *Soft Matter*, 2011, **7**, 1581–1588.
- M. J. Campolongo and D. Luo, *Nat. Mater.*, 2009, **8**, 447–449.
- J. Panyam and V. Labhasetwar, *Adv. Drug Delivery Rev.*, 2003, **55**, 329–347.
- J. M. Anderson and M. S. Shive, *Adv. Drug Delivery Rev.*, 1997, **28**, 5–24.
- H. Li, J. Chang, A. Cao and J. Wang, *Macromol. Biosci.*, 2005, **5**, 433–440.
- J. Yang, W. Tian, Q. Li, Y. Li and A. Cao, *Biomacromolecules*, 2004, **5**, 2258–2268.
- I. Bechthold, K. Bretz, S. Kabasci, R. Kopitzky and A. Springer, *Chem. Eng. Technol.*, 2008, **31**, 647–654.
- R. van Dijkhuizen-Radersma, J. R. Roosma, P. Kaim, S. Metairie, F. L. A. M. A. Péters, J. de Wijn, P. G. Zijlstra, K. de Groot and J. M. Bezemer, *J. Biomed. Mater. Res.*, 2003, **67A**, 1294–1304.
- R. van Dijkhuizen-Radersma, J. R. Roosma, J. Sohler, F. L. A. M. A. Péters, M. van den Doel, C. A. van Blitterswijk, K. de Groot and J. M. Bezemer, *J. Biomed. Mater. Res.*, 2004, **71A**, 118–127.
- L. Wang, J. Chen, H. Liu, Z. Chen, Y. Zhang, C. Wang and Z. Feng, *Polym. Int.*, 2004, **53**, 2145–2154.
- A. Lindström, A. C. Albertsson and M. Hakkarainen, *Polym. Degrad. Stab.*, 2004, **83**, 487–493.
- J. Bremer and H. Osmundsen, *Fatty acid oxidation and regulation*, Amsterdam, Elsevier, 1984.
- J. P. Jain, M. Sokolsky, N. Kumar and A. J. Domb, *Polym. Rev.*, 2008, **48**, 156–191.
- A. J. Domb and M. Maniar, *J. Polym. Sci., Part A: Polym. Chem.*, 1993, **31**, 1275–1285.
- P. Prowans, M. El Fray and J. Slonecki, *Biomaterials*, 2002, **23**, 2973–2978.

- 24 M. Renke-Gluszko and M. El Fray, *Biomaterials*, 2004, **25**, 5191–5198.
- 25 M. El Fray, M. Feldmann, G. Ziegler and P. Prowans, *J. Mater. Sci.: Mater. Med.*, 2007, **18**, 501–506.
- 26 M. El Fray, *Adv. Eng. Mater.*, 2009, **11**, B35–40.
- 27 M. El Fray, A. Piegat and P. Prowans, *Adv. Eng. Mater.*, 2009, **11**, B200–203.
- 28 A. Kozłowska, D. Gromadzki, M. El Fray and P. Štěpánek, *Fib. Text. East Eur.*, 2008, **71**, 85–88.
- 29 E. Jäger, C. G. Venturini, F. S. Poletto, L. M. Colomé, J. P. U. Pohlmann, A. Bernardi, A. M. O. Battastini, S. S. Guterres and A. R. Pohlmann, *J. Biomed. Nanotechnol.*, 2009, **5**, 130–63.
- 30 S. Hornig, T. Heinze, R. Becer and U. S. Schubert, *J. Mater. Chem.*, 2009, **19**, 3838–3840.
- 31 I. Y. Perevyazko, J. T. Delaney Jr, A. Vollrath, G. M. Pavlov, S. Schubert and U. S. Schubert, *Soft Matter*, 2011, **7**, 5030–5035.
- 32 S. A. Galindo-Rodríguez, P. François, S. Briçon, E. Allémann, E. Doelker and H. Fessi, *Eur. J. Pharm. Sci.*, 2005, **25**, 357–367.
- 33 M. Netopilík, F. Schallausky, S. Reichelt, A. Lederer and P. Kratochvíl, *Int. J. Polym. Anal. Charact.*, 2007, **12**, 285–284.
- 34 P. Štěpánek, *J. Chem. Phys.*, 1993, **99**, 6384–6393.
- 35 J. Jakes, *Czech. J. Phys.*, 1988, **38**, 1305.
- 36 P. Štěpánek and Č. Koňák, *Polymer*, 1984, **21**, 195–274.
- 37 J. Kohlbrecher, Software Package SASfit for Fitting Small-Angle Scattering Curves, <http://kur.web.psi.ch/sans1/SANSSoft/sasfit.html>, 2010.
- 38 E. Penott-Chang, A. Walther, P. Millard, A. Jäger, E. Jäger, A. H. E. Müller, S. S. Guterres and A. R. Pohlmann, *J. Biomed. Nanotech.*
- 39 J. M. Chan, L. Zhang, K. P. Yuet, G. Liao, J.-W. Rhee, R. Langer and O. C. Farokhzad, *Biomaterials*, 2009, **30**, 1627–1634.
- 40 F. C. Giacomelli, P. Štěpánek, C. Giacomelli, V. Schmidt, E. Jäger, A. Jäger and K. Ulbrich, *Soft Matter*, 2011, **7**, 9316–9325.
- 41 J. Aubry, F. Ganachaud, J.-P. C. Addad and B. Cabane, *Langmuir*, 2009, **25**, 1970–1979.
- 42 J. Rieger, H. Freichels, A. Imberty, J.-L. Putaux, T. Delair, C. Jérôme and R. Auzély-Velty, *Biomacromolecules*, 2009, **10**, 651–657.
- 43 V. Mailander and K. Landfester, *Biomacromolecules*, 2009, **10**, 2379–2400.
- 44 J. M. Chan, L. Zhang, R. Tong, G. Ghosh, W. Gao, G. Liao, K. P. Yuet, D. Gray, J. Rhee, J. Cheng, G. Golomb, P. Libby, R. Langer and O. C. Farokhzad, *Proc. Natl. Acad. Sci. U. S. A.*, 2010, **107**, 2213–2218.
- 45 P. Štěpánek, in *Dynamic light scattering: The Method and Some Applications*, ed. W. Brown, Oxford Science Publications, Oxford, 1993.
- 46 A. Besheer, J. Vogel, D. Glanz, J. Kressler, T. Groth and K. Mäder, *Mol. Pharmaceutics*, 2009, **6**, 407–415.
- 47 A. Jäger, V. Stefani, S. S. Guterres and A. R. Pohlmann, *Int. J. Pharm.*, 2007, **338**, 297–305.
- 48 M. Seldák and Č. Koňák, *Macromolecules*, 2009, **42**, 7430–7438.
- 49 M. Li, M. Jiang, L. Zhu and C. Wu, *Macromolecules*, 1997, **30**, 2201–2203.
- 50 F. C. Giacomelli, I. C. Riegel, C. L. Petzhold, N. P. Silveira and P. Štěpánek, *Langmuir*, 2009, **25**, 731–738.
- 51 W. Burchard, K. Kajiwara and D. Nерger, *J. Polym. Sci., Polym. Phys. Ed.*, 1982, **20**, 157–171.
- 52 K. Kajiwara, *Polymer*, 1971, **12**, 57–66.
- 53 W. Burchard, in *Light Scattering from Polymers*, ed. W. Burchard, G. D. Patterson, *Advances in Polymer Science*, 48, Springer-Verlag, New York, 1983; pp. 66–78.
- 54 J. Fu and C. Wu, *J. Polym. Sci., Part B: Polym. Phys.*, 2001, **39**, 703–708.
- 55 J. Fu, X. Li, D. K. P. Ng and C. Wu, *Langmuir*, 2002, **18**, 3843–3847.
- 56 Č. Koňák, V. Šubr, L. Kostka, S. Štěpánek, K. Ulbrich and H. Schlaad, *Langmuir*, 2008, **24**, 7092–7098.
- 57 F. Quaglia, L. Ostacolo, G. De Rosa, M. I. La Rotonda, M. Ammendola, G. Nese, G. Maglio, R. Palumbo and C. Vauthier, *Int. J. Pharm.*, 2006, **324**, 56–66.
- 58 L. A. Fiel, L. M. Rebêlo, T. M. Santiago, M. D. Adorne, S. S. Guterres, J. S. Sousa and A. R. Pohlmann, *Soft Matter*, 2011, **7**, 7240–7247.
- 59 J. Panyam, D. Williams, A. Dash, D. Leslie-Pelecky and V. Labhasetwar, *J. Pharm. Sci.*, 2004, **93**, 1804–1814.
- 60 Y. Tu, X. Wan, D. Zhang, Q. Zhou and C. Wu, *J. Am. Chem. Soc.*, 2000, **122**, 10201–10205.
- 61 Y. Zhao, J. Fu, D. K. P. Ng and C. Wu, *Macromol. Biosci.*, 2004, **4**, 901–906.
- 62 F. von Burkersroda, L. Schedl and A. Göpferich, *Biomaterials*, 2002, **23**, 4221–4231.
- 63 G. Wei, Y. Li, G. Du and J. Chen, *Process Biochem.*, 2003, **38**, 1133–1138.